ELSEVIER

Mathematical Biosciences 153 (1998) 99–124

Mathematical Biosciences
an international journal

Consequences of population models for the dynamics of food chains

B.W. Kooi *, M.P. Boer, S.A.L.M. Kooijman

Faculty of Biology, Free University, De Boelelaan 1087, 1081 HV Amsterdam, The Netherlands

Received 11 February 1998; received in revised form 21 July 1998

Abstract

A class of bioenergetic ecological models is studied for the dynamics of food chains with a nutrient at the base. A constant influx rate of the nutrient and a constant efflux rate for all trophic levels is assumed. Starting point is a simple model where prey is converted into predator with a fixed efficiency. This model is extended by the introduction of maintenance and energy reserves at all trophic levels, with two state variables for each trophic level, biomass and reserve energy. Then the dynamics of each population are described by two ordinary differential equations. For all models the bifurcation diagram for the bi-trophic food chain is simple. There are three important regions; a region where the predator goes to extinction, a region where there is a stable equilibrium and a region where a stable limit cycle exists. Bifurcation diagrams for tri-trophic food chains are more complicated. Flip bifurcation curves mark regions where complex dynamic behaviour (higher periodic limit cycles as well as chaotic attractors) can occur. We show numerically that Shil'nikov homoclinic orbits to saddle-focus equilibria exists. The codimension 1 continuations of these orbits form a 'skeleton' for a cascade of flip and tangent bifurcations. The bifurcation analysis facilitates the study of the consequences of the population model for the dynamic behaviour of a food chain. Although the predicted transient dynamics of a food chain may depend sensitively on the underlying model for the populations, the global picture of the bifurcation diagram for the different models is about the same.

Keywords: Bifurcation analysis; Chemostat; Food chain; Chaos; Shil'nikov homoclinic bifurcation

* Corresponding author. Tel.: +31-20 444 7129; fax: +31-20 444 7123; e-mail: kooi@bio.vu.nl

0025-5564/98/$ – see front matter
PII: S0025-5564(98)10037-8

1. Introduction

A commonly used model for ecosystems is the Rosenzweig–MacArthur model [1]. This model differs from the classical Lotka–Volterra model in that a linear functional response is replaced by the Holling type II functional response. The modelled ecosystem might consist of plants, herbivore and carnivores, for instance phytoplankton, zooplankton and fish, where carnivores consume herbivores and herbivores consume plants. The dynamic behaviour of the Rosenzweig–MacArthur model has been studied extensively in the literature. Rosenzweig and MacArthur gave a graphical representation of the qualitative aspects of the dynamics of a general type of a bi-trophic [2] and a tri-trophic food chain [3]. Gragnani and Rinaldi dealt with persistence and also stability conditions for equilibria were discussed. The abundance of the top predator in these food chains under various environmental conditions, especially enrichment of the nutrient, has been studied in [1,4]. In [5] a resource, consumer and predator model, derived from a bioenergetic model but mathematically equivalent with the Rosenzweig–MacArthur model, was presented and analysed. The parameters of this model were derived in [6] from allometric and energetic relations. McCann and Yodzis also exploited zero isoclines or null-surfaces for the study of the dynamics of this tri-trophic food chain. In [5,7–10] bifurcation analysis is applied to the Rosenzweig–MacArthur model. Various types of complex dynamics, including chaotic behaviour, were found.

The lowest level in the Rosenzweig–MacArthur model is self-reproducing with logistic growth. This implies hidden assumptions about the nutrient availability. In the bioenergetic food chain models discussed in the present paper, non-reproducing nutrients at the base are modelled explicitly. These models obey mass conservation laws and will be called mass-balance models. These models can be formulated for various environmental conditions. In this paper a continuous flow culture with constant influx of nutrients and constant dilution rate for all trophic levels is assumed. These homogeneous environmental conditions hold for wastewater treatments plants, but also for the chemostat, a laboratory arrangement commonly employed in the study of the growth kinetics of microbial cell populations. The chemostat experiments can also be carried out in order to mimic the interactions going on in a lake or in a marine environment [11].

The Monod model [12] is classical in the dynamics of populations consisting of unicellular microorganisms which propagate by binary fission. In that model food is ingested at a rate given by the Holling type II functional response. A fixed portion of the ingested food is used for growth.

In a variant of the Monod model, the Monod–Herbert or Marr–Pirt model [13], ingested food is not only used for growth but also for maintenance. The maintenance costs are proportional to the biomass of the population. In an other variant of the Monod model, Droop [14,15] introduced the concept of

cell nutrient quota in a model for phytoplankton growth. Ingested food is converted into internal reserves, while growth depends on the amount of reserves. These reserves impose a kind of inertia on the response to changing food conditions. In [15] the global stability of the Droop equations with a single species in the chemostat has been investigated mathematically.

The Dynamic Energy Budget (DEB) model proposed by Kooijman [16] also takes both maintenance costs and energy reserves into account. In the former respect the DEB model is similar to the Marr–Pirt model and in the latter it resembles the Droop model. Besides the biomass the density of the energy reserves is also presented as a state variable. For species which propagate by binary fission a population dynamic model has been derived from the dynamics of the individuals in [17]. For species with complex physiology or with a number of life stages (egg, embryo, juvenile or adult) the connection between the individual level and the population level is much more involved [18]. The variables which describe the state of the population are weighted averages of those of the individuals that make up the population. In those cases the mathematical description of the dynamics of the population with a set of ordinary instead of partial differential equations may be rather crude. The same applies, however, to all unstructured population models, including the logistic growth model, the Lotka–Volterra model and the Rosenzweig–MacArthur model.

Cunningham and Nisbet [19,20] studied the dynamic behaviour of a bi-trophic microbial food chain consisting of substrate, bacterium and ciliate in a chemostat. They used the Marr–Pirt model and showed that the introduction of maintenance has a stabilizing effect, especially for low dilution rates. In [21] and [22] the complex dynamics of a forced bi-trophic microbial food chain in a chemostat with forcing in the form of a periodic influx of substrate has been discussed.

The periodically forced Rosenzweig–MacArthur model besides that of the mass-balance model is studied in [11]. They concluded that all basic modes of behaviour of the two best studied predator-prey models (the Rosenzweig–MacArthur and the mass-balance model) can be explained by means of a single bifurcation diagram in which quasi-periodicity, phase locking, periodic doubling and chaotic dynamical behaviour are indicated.

We will analyse the consequences of four different models for the population level on the long-term dynamic behaviour of an autonomous food chain: Monod, Marr–Pirt, Droop and DEB. These models are formulated in Section 2. The bifurcation diagrams with the dilution rate and concentration of the substrate in the influx as free parameters are presented and discussed in Section 3.1. The results were obtained with different general-purpose bifurcation computer software packages, AUTO [23,24] and LOCBIF[25]. In Section 3.2 the consequences of the introduction of maintenance on the dynamic behaviour of the food chain for small dilution rates are studied. For the Droop

model a subcritical flip bifurcation occurs in a very small region of the bifurcation parameter space. This phenomenon is studied in Section 3.3.

A homoclinic Shil'nikov bifurcation in the biologically interesting region of the parameter space for all models except the Monod model, is described in Section 4. This type of global bifurcation is discussed for instance in [26–28]. The homoclinic bifurcations were calculated with the packages HOMCONT [29], implemented in AUTO [24]. Other types of global bifurcations for the Marr–Pirt model were already described in [30]. Global bifurcations form a skeleton for the period doubling of which a cascade leads to chaotic dynamics.

2. Description of the models

This section presents the DEB model and the Marr–Pirt model, whereas the Droop model and the Monod model are obtained as special cases; see also Table 1. Let $x_0(t)$ denote the density of the resource (nutrient, substrate). Furthermore, let $x_i(t)$, $i=1, 2, 3$ denote biomass densities of prey, predator and top predator, respectively, and $e_i(t)$, $i=1, 2, 3$ denote scaled reserve densities. A scaled energy density is defined as the energy density divided by the maximum energy density, which is assumed to be a species specific parameter. Thus the subindex indicates the population level, where index $i=0$ denotes the non-viable resource level. When two population levels are involved in the definition of a parameter, two sub-indices will be used. For instance, $f_{i-1,i}$ denotes the scaled Holling type II functional response with saturation constant $k_{i-1,i}$ given by

$$f_{i-1,i} = \frac{x_{i-1}}{k_{i-1,i} + x_{i-1}}, \quad i = 1, 2, 3 \tag{1}$$

and this models feeding of the i-population on the $(i-1)$-population.

The DEB model reads

$$\frac{\mathrm{d}x_0}{\mathrm{d}t} = (x_r - x_0)D - I_{0,1} f_{0,1} x_1, \tag{2a}$$

$$\frac{\mathrm{d}x_i}{\mathrm{d}t} = x_i \frac{v_{i-1,i} e_i - m_i g_i}{e_i + g_i} - D x_i - I_{i,i+1} f_{i,i+1} x_{i+1}, \quad i = 1, 2, \tag{2b}$$

Table 1
Classification of the different population models

Reserves	No $g_i = \infty, v_{i-1,i} = \infty$ while $v_{i-1,i}/g_i = \mu_{i-1,i}$	Yes
Maintenance		
No, $m_i = 0$	Monod	Droop
Yes	Marr–Pirt	DEB

$$\frac{dx_3}{dt} = x_3 \frac{v_{2,3}e_3 - m_3 g_3}{e_3 + g_3} - Dx_3, \tag{2c}$$

$$\frac{de_i}{dt} = v_{i-1,i}(f_{i-1,i} - e_i), \quad i = 1, 2, 3. \tag{2d}$$

The last term at the right-hand sides of Eq. (2a) and Eq. (2b) represents the depletion rate due to predation proportional to the predator biomass density x_i. Here $I_{i-1,i}$ is the maximum ingestion rate. This ingestion rate is attained when $f_{i-1,i} \to 1$ that is, when there is abundant food.

The first terms at the right-hand sides of system (2a–2d) are growth terms proportional to biomass density x_i. Finally there are terms representing the efflux Dx_i, $i = 1, 2, 3$ for all trophic levels. For the top predator this is the only source of depletion. Eq. (2d) is a constitutive relationship which states that the energy reserve density dynamics follows food dynamics via a first order process, where the constant of proportionality is the energy conductance rate $v_{i-1,i}$. When there are no costs for maintenance, system (2a–2d), reduces to the Droop model [14]. However, this model is now used for other organisms than phytoplankton as well, for instance zooplankton with a complicated life cycle. For a complete description of the model and the biological meaning of the parameters the reader is referred to [16] as well as Table 2.

Without reserves the model is equivalent to the Marr–Pirt model [31]. This model reads

Table 2
Parameters and state variables; t = time, m = biomass, v = volume of the reactor. The subindex denotes the trophic level, $i = 0$ substrate, $i = 1$ bacteria, $i = 2$ ciliate and $i = 3$ carnivore. Some parameters, for instance the saturation constants $k_{i-1,i}$, have double sub-indexes to emphasize that these quantities depend on two levels

Parameter	Dimension	Units	Interpretation
D	t^{-1}	h^{-1}	Dilution rate
e_i	–	–	Scaled energy reserve density
$f_{i-1,i}$	–	–	Scaled functional response
g_i	–	–	Energy investment ratio, $\propto$ costs for growth
$I_{i-1,i}$	t^{-1}	h^{-1}	Maximum food uptake rate
$k_{i-1,i}$	m v^{-1}	mg dm^{-3}	Saturation constant
m_i	t^{-1}	h^{-1}	Maintenance rate coefficient
t	t	h	Time
T_0	t	h	Period of the limit cycles
x_0	m v^{-1}	mg dm^{-3}	Substrate density
x_i	m v^{-1}	mg dm^{-3}	Biomass density
x_r	m v^{-1}	mg dm^{-3}	Substrate concentration in reservoir
$y_{i-1,i}$	–	–	Maximum yield
$\mu_{i-1,i}$	t^{-1}	h^{-1}	Maximum population growth rate
$v_{i-1,i}$	t^{-1}	h^{-1}	Energy conductance, $\propto$ assimilation rate

$$\frac{dx_0}{dt} = (x_r - x_0)D - I_{0,1}f_{0,1}x_1\ , \tag{3a}$$

$$\frac{dx_1}{dt} = \mu_{0,1}f_{0,1}x_1 - D_1x_1 - I_{1,2}f_{1,2}x_2, \tag{3b}$$

$$\frac{dx_2}{dt} = \mu_{1,2}f_{1,2}x_2 - D_2x_2 - I_{2,3}f_{2,3}x_3, \tag{3c}$$

$$\frac{dx_3}{dt} = \mu_{2,3}f_{2,3}x_3 - D_3x_3, \tag{3d}$$

where D_i, is the depletion rate. In our case we will assume that depletion is due to two effects, namely $D_i = D + m_i$, where D is the rate at which all trophic levels are exported and m_i the maintenance rate coefficient and/or the natural death or harvesting rate. The link with the DEB model, system (2a–2d), is obvious when we require $g_i \to \infty$ and $v_{i-1,i} \to \infty$ while $v_{i-1,i}/g_i = \mu_{i-1,i}$, where $\mu_{i-1,i}$ is the maximum growth rate at the ith trophic level, while $f_{i-1,i}(t) = e_i(t)$ for $i = 1, 2, 3$. The system (3a–3d) resembles the Rosenzweig–MacArthur model often used to describe the dynamics of ecosystems.

When furthermore in system (3a–3d) $m_i = 0$, $i = 1, 2, 3$ or $D_1 = D_2 = D_3 = D$, the system becomes Monod's model [12]. In the Monod model there is no maintenance nor natural death and a fixed part of the ingested food (expressed in mass or an equivalent amount of energy) is converted into biomass, at a constant yield $y_{i-1,i} = \mu_{i-1,i}/I_{i-1,i}$. As a consequence it is possible to decouple the system (3a–3d) by introduction of the function

$$H(t) = y_{0,1}y_{1,2}y_{2,3}(x_0(t) - x_r) + y_{1,2}y_{2,3}x_1(t) + y_{2,3}x_2(t) + x_3(t), \quad t \geqslant 0. \tag{4}$$

It is easy to show that

$$\frac{dH}{dt} = -DH. \tag{5}$$

The biological interpretation of the $-DH$ term is the difference between the influx rate and the outflux rate of the total biomass expressed in the biomass of the top predator. In [32] Eq. (5) is used to show that Monod's model is dissipative and that the system converges asymptotically to the manifold $H = 0$ where the influx rate and outflux rate of the total biomass are the same.

3. Bifurcation analysis

Bifurcation analysis gives information about the long-term dynamic behaviour of non-linear dynamic systems, that is the asymptotic stability of equilibria, periodic orbits and chaotic attractors. The structural stability is studied with respect to so-called free or bifurcation parameters, [26,28]. If an attractor changes character or disappears completely under slight adjustment

Table 3
List of all bifurcations, codimension-one curves and codimension-two points

Bifurcation	Description
	Codim-1 curves
$TC_{e,i}$	Transcritical bifurcation; Invasion by population i through boundary equilibrium.
$TC_{c,i}$	Transcritical bifurcation; Invasion by population i through boundary limit cycle.
H_i^*	Hopf bifurcation: $* = -$ supercritical, $* = +$ subcritical; i-trophic food chain becomes unstable, origin of stable (supercritical) or unstable (subcritical) limit cycle.
$T_{e,i}$	Tangent bifurcation; For equilibrium of i-trophic food chain.
$T_{c,i}$	Tangent bifurcation; For limit cycle of i-trophic food chain.
F_j^*	Flip bifurcation, $j = 1, 2$: $* = -$ supercritical, $* = +$ subcritical; period doubling of limit cycle of tri-trophic food chain.
$G_e^=$	Homoclinic bifurcation; Shil'nikov global bifurcation for equilibrium of tri-trophic food chain.
	Codim-2 points
M_j	Codimension-two bifurcation points, $j = 1, 2, 3$; Bifurcation of transcritical bifurcations of tri-trophic food chain.
L	Bautin bifurcation point; Transition from sub- to supercritical Hopf bifurcation for tri-trophic food chain.
N	Cusp bifurcation point; Bifurcation point for limit cycles of tri-trophic food chain.
P_j	Codimension-two bifurcation points, $j = 1, 2$; Transition from sub- to supercritical flip bifurcation for tri-trophic food chain.

of a free parameter, the system is structurally unstable. The point in the parameter space where this happens is called a bifurcation point. In Table 3 a list of all bifurcation curves and points, and the scheme behind the notation is given.

3.1. Description of the bifurcation diagrams

In this section we describe the (local) bifurcation diagrams of the four different models. The bifurcation parameters are the control parameters which are set by the experimentalist: the dilution rate, D, and the concentration of nutrients in the influx, x_r. In Table 4 the parameter setting is given for a microbial food chain in the chemostat. All bifurcation curves associated with equilibria were calculated with LOCBIF [25,28]. AUTO [23,24] was used for the calculation of the curves associated with limit cycles. These computer programs are implementations of continuation techniques which facilitate the study of the change of the position of the bifurcation points due to a change of free parameters. Starting at a point on a bifurcation curve, this curve is continued while test functions which are indicative of higher codimension bifurcation points are checked.

Table 4
Parameter set for bacterium-ciliate models, after Cunningham and Nisbet [19,20]. The values for the new parameters m_i (equal to 5% of the maximum growth rate $\mu_{i-1,i}$) and g_i are also given. The relationships $I_{i-1,i} = \mu_{i-1,i}/y_{i-1,i}$ and $v_{i-1,i} = \mu_{i-1,i}g_i$ hold true for $i = 1, 2, 3$. The ranges for the control parameters are $0 < D < \mu_{0,1}$ and $0 < x_r \leqslant 300$ mg dm^{-3}

Parameter	Unit	Values		
		$i=1$	$i=2$	$i=3$
$y_{i-1,i}$	–	0.4	0.6	0.6
$\mu_{i-1,i}$	h^{-1}	0.5	0.2	0.15
$k_{i-1,i}$	mg dm^{-3}	8	9	10
$I_{i-1,i}$	h^{-1}	1.25	0.33	0.25
m_i	h^{-1}	0.025	0.01	0.0075
g_i	–	80.0	1.0	0.504
$v_{i-1,i}$	h^{-1}	40.0	0.2	0.0756

A realistic parameter value for the energy investment ratio of the prey is $g_1 = 80$. This implies that $v_{0,1} = 40$ h^{-1} for we have $v_{i-1,i} = \mu_{i-1,i}g_i$ where $\mu_{i-1,i} = 0.5$ h^{-1} (see Table 4). As a result system (2a–2d) is rather stiff due to Eq. (2d), $i = 1$. In order to circumvent numerical problems with continuation, we assumed that the dynamics of the reserves of the prey is quasi-static, that is $e_1(t) = f_{0,1}(t)$. This reduces the dimension from seven to six. The biological justification is that the prey species tends to have a relatively small body size and in [16] it is predicted that reserve turnover rate v increases with decreasing body size. A high turnover rate implies a quasi-steady state.

In Fig. 1 we show the bifurcation diagram for a bi-trophic food chain calculated with Monod's model. The curves $TC_{e,1}$ and $TC_{e,2}$ are transcritical bifurcation curves and H_2^- marks a supercritical Hopf bifurcation curve. There are three important regions; a region where the predator goes to extinction (left-hand side of $TC_{e,2}$), a region with a stable equilibrium (at the right-hand side of $TC_{e,1}$ and at the left-hand side of H_2^-) and a region where a stable limit cycle exists (to the right of H_2^-). The transition over the supercritical Hopf bifurcation curve, H_2^-, due to an increase in the nutrient supply is associated with the paradox of enrichment [2].

In the diagrams for a tri-trophic food chain there is an 'organizing center', namely the codimension 2 point M_1. In Fig. 2 the transcritical curves $TC_{e,3}$ and $TC_{c,3}$ for equilibria and limit cycles where $x_3 = 0$, originating from M_1 are given. These transcritical curves are important with respect to the invasibility of a top predator. On the transcritical bifurcation curves in points M_2 and M_3 tangent bifurcation curves originate for equilibria, $T_{e,3}$ and limit cycles, $T_{c,3}$ respectively. The latter tangent bifurcation curve $T_{c,3}$ has a cusp bifurcation point denoted by N. The bifurcation diagrams for all models have basically this portrait (Figs. 3–6).

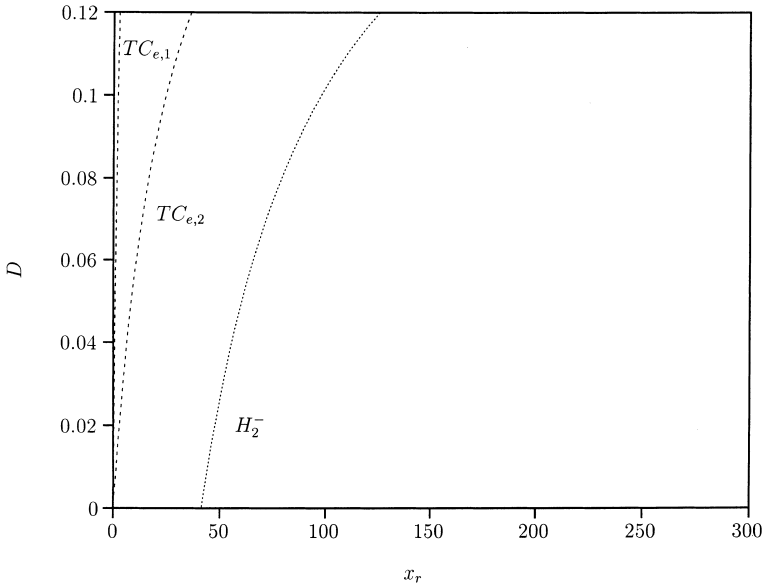

Fig. 1. Bifurcation diagram for Monod's model with two trophic levels: system (3a–3d). The bifurcation parameters are the dilution rate D [h^{-1}] and the substrate concentration in reservoir x_r [mg dm^{-3}]. Values assigned to physiological parameters are listed in Table 4. The curves $TC_{e,1}$ and $TC_{e,2}$ are transcritical bifurcation curves and H_2^- marks a supercritical Hopf bifurcation curve. The latter curve is associated with the paradox of enrichment.

The codimension 2 point, M_1, is the intersection point of the supercritical Hopf bifurcation curve H_2^- and the transcritical bifurcation curve for equilibria $TC_{e,3}$ (Fig. 3). Furthermore in this point M_1 a subcritical Hopf bifurcation curve, H_3^+, originates. Without energy reserves (Monod and Marr–Pirt) the curve $TC_{c,3}$ intersects the Hopf bifurcation curve H_3^+ in point M_1 (Figs. 3 and 4).

The bifurcation diagrams for the Droop and the DEB model, differ from that of the Monod and Marr–Pirt model, respectively, in the vicinity of the codimension 2 point M_1 (Figs. 5 and 6). Namely, with reserves the Hopf bifurcation curve starts supercritically, $H_{3_2}^-$, and becomes subcritical, H_3^+, at the Bautin bifurcation point L. Furthermore the curve $TC_{c,3}$ now intersects the Hopf bifurcation curve $H_{3_2}^-$ at a point apart from point M_1. There is a tangent bifurcation curve for interior limit cycles which originates at the Bautin bifurcation point L. This tangent bifurcation curve (not shown in the figures) is tangent to the transcritical curve $TC_{c,3}$ where it lies at the boundary of the state space where $x_3(t) = 0$. The dynamics in the region around point M_1 are described in more detail elsewhere [33].

Furthermore, with reserves there are two period-1 $\rightarrow$ 2 flip bifurcation curves F_1 and F_2 which intersect each other as shown in Figs. 5 and 6. Observe

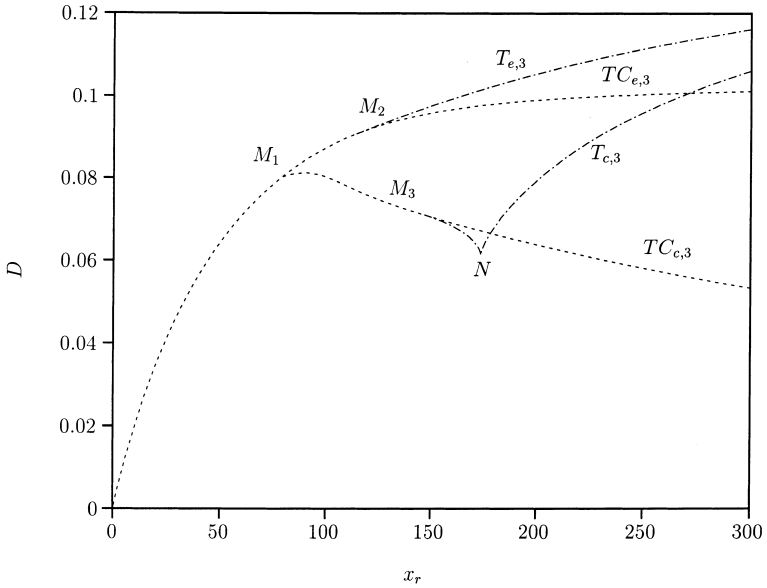

Fig. 2. Detail of the bifurcation diagrams around the organizing center M_1 with only transcritical and tangent bifurcation curves. $TC_{e,3}$ marks a transcritical bifurcation and $T_{e,3}$ marks a tangent bifurcation curve both for equilibria. These curves originate in codimension 2 point M_2. $TC_{c,3}$ marks a transcritical bifurcation with $x_3 = 0$ and $T_{c,3}$ tangent bifurcation curve, both for limit cycles. These both curves originate in the codimension 2 point M_3. There is a cusp bifurcation point denoted by N for the curve $T_{c,3}$.

that the intersection points are not codimension 2 points. There is just coexistence of two stable limit cycles. Inside the region bounded by the Hopf bifurcation curve, H_3^-, a cascade of period doubling leads to chaotic behaviour. This holds for all models.

3.2. Comparison of the bifurcation diagrams

Comparison of the four diagrams (Figs. 3–6) reveals that for small dilution rates the influence of maintenance in the dynamic behaviour is significant. Without maintenance (Monod and Droop model) the codimension 1 curves (transcritical $TC_{e,1}$, $TC_{e,2}$ and $TC_{e,3}$ and the supercritical Hopf bifurcation curves H_2^- and H_3^-) approach the x_r-axis, while with maintenance this axis is a horizontal asymptote for these curves. Stated otherwise, in the first two models with $D > 0$, there is an interior equilibrium or an interior stable limit cycle for the full-length food chain. For small D-values, the period of the periodic orbits becomes very large and the state variables become very small over part of the

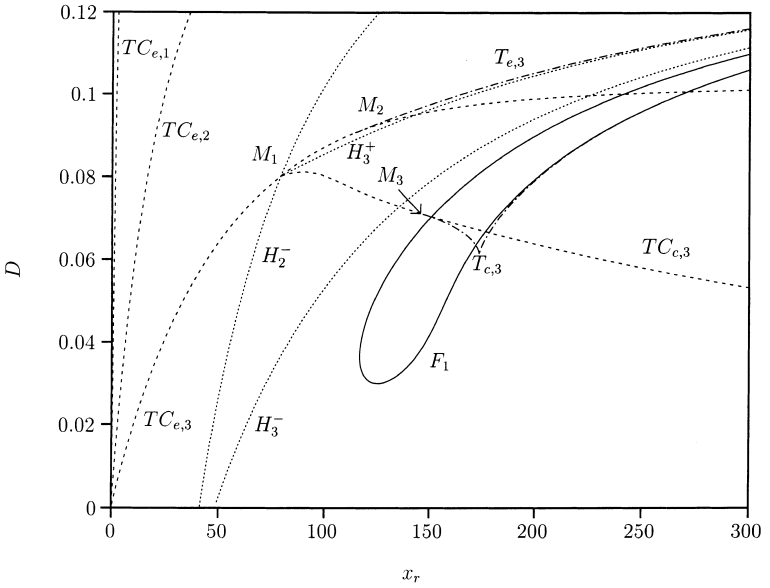

Fig. 3. Bifurcation diagram for Monod's model (system (3a–3d) with $m_i = 0$ for $i = 1, 2, 3$). The bifurcation parameters are the dilution rate D [h^{-1}] and the substrate concentration in reservoir x_r [mg dm^{-3}]. Dotted curves H_2^-, H_3^+ and H_3^- mark Hopf bifurcations. The curves $TC_{e,1}$, $TC_{e,2}$, $TC_{e,3}$ mark transcritical bifurcation curves for equilibria and $TC_{c,3}$ marks a transcritical bifurcation curve for limit cycles. Curves $T_{e,3}$ and $T_{c,3}$ mark tangent bifurcation curves for equilibria and limit cycles, respectively. There is a period-1 $\rightarrow$ 2 flip bifurcation curve F_1.

orbit. An important consequence is that the food chain can become partly extinct during these periods due to stochastic fluctuations.

On the contrary, in the two models with maintenance (Marr–Pirt and DEB model) only the population at the lowest trophic level survives when D becomes small. This shows that the introduction of maintenance, mathematically described by the introduction of a term in the numerator for the growth rate term, Eqs. (2b) and (2c) , is extremely important for small D values. From a bifurcation analysis point of view the Marr–Pirt and DEB models are derived from the Monod and Droop models, respectively, by changing the three parameters m_i; in our case only one parameter $\rho = m_i g_i / v_{i-1,i}, i = 1, 2, 3$. Comparison of Figs. 4 and 6 with the Figs. 3 and 5, respectively, shows that there is a strong dependency with respect to ρ when $\rho \downarrow 0$. Although the dependency of the right-hand sides of the ODEs with respect to ρ is smooth for $\rho \downarrow 0$, the codimension 1 curves in the bifurcation diagram depend largely on ρ for very small D values. Observe that with $D = 0$ the bifurcation diagram degenerates, for the parameter x_r is then redundant because there is no influx of substrate. So, only asymptotic behaviour, $\lim D \downarrow 0$, is relevant. For the models where

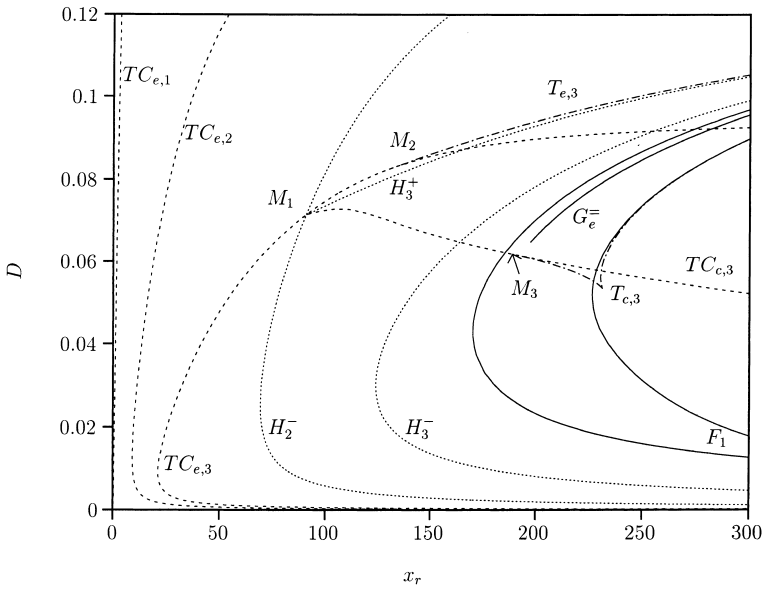

Fig. 4. Bifurcation diagram for the Marr–Pirt model (system (3a–3d)). The bifurcation parameters are the dilution rate D [h^{-1}] and the substrate concentration in reservoir x_r [mg dm^{-3}]. For an explanation of the symbols see Fig. 3. The curve $G_e^=$ marks a global homoclinic bifurcation to the unstable equilibrium.

$\rho > 0$ all populations except the lowest trophic level go extinct for infinitesimal small D, while for models with $\rho = 0$ the interior solutions at the left side of the Hopf bifurcation lines H_2^- or H_3^- converge smoothly to an interior equilibrium point or limit cycle.

This can be shown analytically for the transcritical bifurcation curve $TC_{e,2}$ of system (3a–3d) for the bi-trophic food chain as follows. On the transcritical bifurcation curve we have

$$0 = (x_r - x_0)D - I_{0,1}f_{0,1}x_1, \tag{6a}$$

$$0 = \mu_{0,1}f_{0,1} - D_1, \tag{6b}$$

$$0 = \mu_{1,2}f_{1,2} - D_2. \tag{6c}$$

The first two Eqs. (6a) and (6b) are just equilibrium equations for the bi-trophic food chain and Eq. (6c) fixes the transcritical bifurcation.

The explicit expression of x_r as function of D becomes after some algebraic manipulations

$$x_r = \frac{(D + m_1)k_{0,1}}{\mu_{0,1} - D - m_1} + \frac{1}{D}\frac{I_{0,1}(D + m_1)(D + m_2)k_{1,2}}{\mu_{0,1}(\mu_{1,2} - D - m_2)}. \tag{7}$$

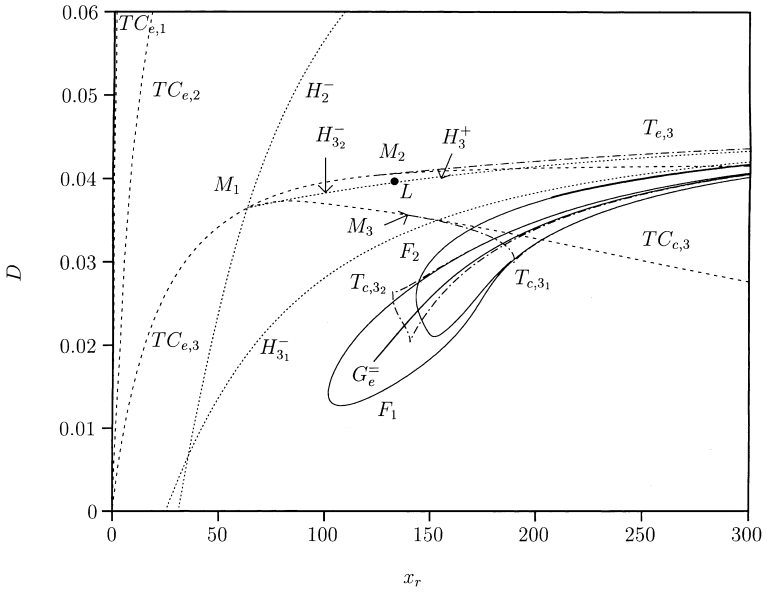

Fig. 5. Two-parameter bifurcation diagram for the Droop model, (system (2a–2d) with $m_i = 0$ for $i = 1, 2, 3$). The bifurcation parameters are the dilution rate D [h^{-1}] and the substrate concentration in reservoir x_r [mg dm^{-3}]. For an explanation of the symbols see Fig. 3. Subcritical and supercritical Hopf bifurcations, H_3^+ and $H_{3_2}^-$, respectively, are now distinguished. Point L is a Bautin bifurcation point. There is an extra tangent bifurcation curve, $T_{c,3_2}$, for limit cycles. This curve marks a region with multiple limit cycles. There is also a period-1 $\rightarrow$ 2 flip bifurcation curve F_2.

This shows that

$$\text{if} \quad m_1 = m_2 = 0 \qquad \text{then} \qquad \lim_{D \downarrow 0} x_r = 0, \tag{8}$$

$$\text{if} \quad m_1 > 0, m_2 > 0 \qquad \text{then} \qquad \lim_{D \downarrow 0} x_r = \infty. \tag{9}$$

The graph of the function $x_r(D)$ given by Eq. (7) is the transcritical bifurcation curve $TC_{e,2}$ in Figs. 3 and 4.

The first term at the right-hand side describes the transcritical bifurcation curve $TC_{e,1}$. The dependency for $D \downarrow 0$ with respect to m_1 is then smooth; the curve $TC_{e,1}$ terminates in $x_r = m_1 k_{0,1}/(\mu_{0,1} - m_1)$. However, with maintenance we have for the biomass density $x_1 \rightarrow 0$ if $D \downarrow 0$. Without maintenance costs the single species remains in the chemostat also for infinitesimal small dilution rates.

Nisbet et al. [20], in studying the bi-trophic food chain, took the maintenance of the lowest trophic level zero as in the Monod model; only maintenance for the predator was introduced. The resulting bifurcation diagram shows persistence (interior stable equilibrium) when D becomes infinitesimally

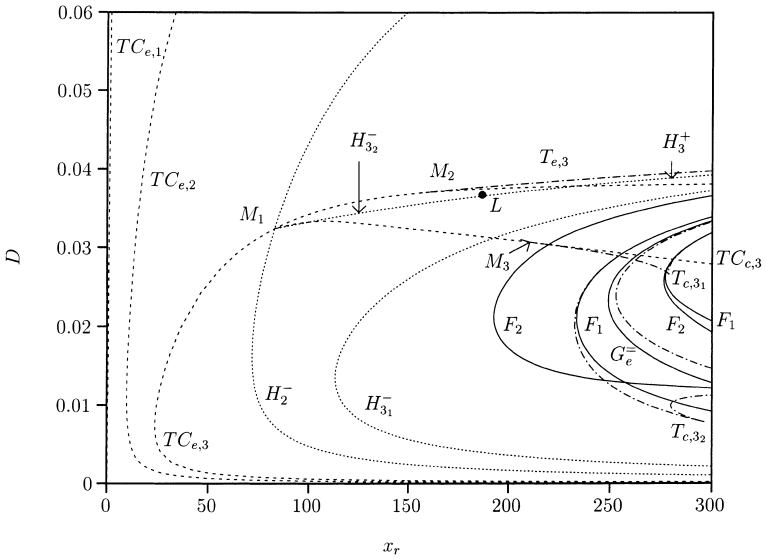

Fig. 6. Bifurcation diagram for the DEB model (system (2a–2d)). The bifurcation parameters are the dilution rate D [h^{-1}] and the substrate concentration in reservoir x_r [mg dm^{-3}]. For an explanation of the symbols see Figs. 3 and 5.

small. Then the transcritical bifurcation curve $TC_{e,2}$ terminates at the x_r-axis as it does in the Monod model (Fig. 3). This follows also from Eq. (7)

$$\text{if} \qquad m_1 = 0, m_2 > 0 \qquad \text{then} \qquad \lim_{D \downarrow 0} x_r = I_{0,1} D_2 k_{1,2} / (\mu_{0,1}(\mu_{1,2} - D_2)). \tag{10}$$

Nevertheless, the Hopf bifurcation curve H_2^- bends to the x_r-axis for $x_r \to \infty$, as in the Marr–Pirt model (Fig. 4).

Invasion of a species is possible when its growth rate is larger then the depletion rate. This yields an upperbound for the dilution rate where the food chain can persist. At equilibrium where $e_i(t) = f_{i-1,i}(t)$, $i = 1, 2, 3$, the growth rate term $\mathscr{M}_{i-1,i}$ reads

$$\mathscr{M}_{i-1,i} = \frac{v_{i-1,i} f_{i-1,i} - m_i g_i}{f_{i-1,i} + g_i} \quad \Rightarrow \quad \mathscr{M}_{i-1,i}\Big|_{f_{i-1,i}=1} = \frac{\mu_{i-1,i} - m_i}{1/g_i + 1}. \tag{11}$$

The maximum attainable growth rate, i.e. the growth rate at abundant food ($f_{i-1,i} = 1$), is smaller than the maximum growth rate in the Monod model, $\mu_{i-1,i}$, for two reasons, namely maintenance costs (term $-m_i < 0$) and having energy reserves (factor $1/(1/g_i + 1) < 1$). We took maintenance proportional to the maximum growth rate, $v_{i-1,i}/g_i$, for all trophic levels, so there is only one extra parameter, denoted by ρ and defined by $m_i = \rho v_{i-1,i}/g_i$. Because of the

assumption that the maintenance rate coefficient is $m_i = 0.05\mu_{i-1,i}$, the maximum attainable growth rate diminishes by 5%. For the Marr–Pirt model Eq. (7) shows that with $D \to \mu_{1,2} - m_2$ or $D \to \mu_{0,1} - m_1$ we have $x_r \to \infty$.

When the cost for growth is rather low the costs for reserve synthesis tend to dominate. The investment ratio for the top predator has been set at $g_3 = 0.504$ and therefore the maximum attainable growth rate is reduced by a factor of about one third compared to the Monod model. Organisms with reserves can sustain periods of starvation rather well but their maximum attainable growth rate is much smaller. This reduction implies that in the (x_r, D)-plane the full food chain persists in a smaller region for the DEB model than for the Monod model.

3.3. Subcritical flip bifurcation

In Fig. 7 a detail of the bifurcation diagram for the Droop model (Fig. 5) is given. In this plot also flip and tangent bifurcations with higher order periodicity are shown. There now is a tangent bifurcation of period-2 limit cycles denoted as $T_{c,3_3}$. This tangent bifurcation is connected to a subcritical flip

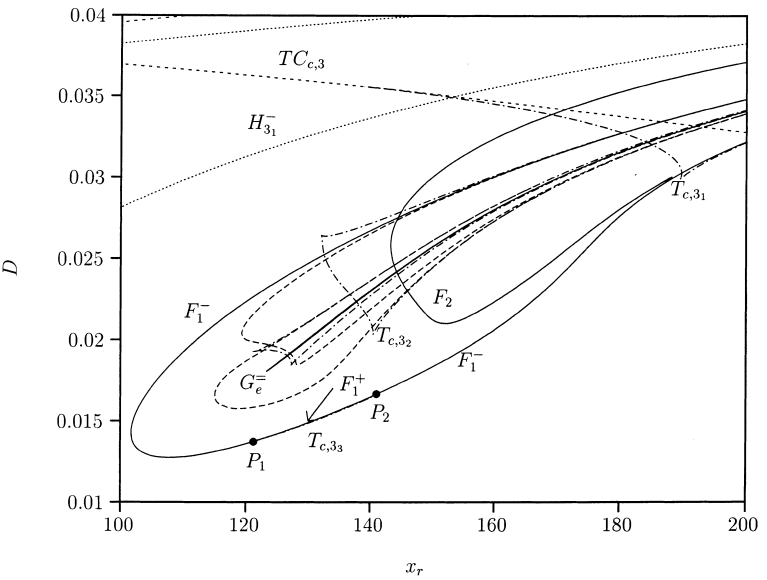

Fig. 7. Two-parameter bifurcation diagram for the Droop model (system (2a–2d) with $m_i = 0$ for $i = 1, 2, 3$). This figure is an expanded picture of Fig. 5. For an explanation of the symbols see Fig. 3. Subcritical and supercritical flip bifurcations, F_1^+ and F_1^- respectively, are now distinguished. The points P_1 and P_2 are transition points from subcritical to supercritical for the flip bifurcation denoted by F_1. Between these points there is a tangent bifurcation of period-2 limit cycles, $T_{c,3_3}$.

bifurcation. In order to study these bifurcations we consider now one-parameter diagrams. In these diagrams, for a fixed x_r, the peak values of the top predator is shown as a function of the free parameter, the dilution rate D. The system is integrated in time starting from perturbed equilibria (the equilibrium value for the top predator was increased slightly). In case of multiple limit cycles or chaotic attractors, the system starts from the attractor for slightly different values of D in a continuation process. In order to get rid of the transients, integration is performed for a fixed time without examination of the results. From that point in time the top predator peak value is shown as a dot in the diagram.

In Fig. 8 the long-term peak values for x_3 are displayed, where $x_r = 140$ mg dm^{-3}. For small D values the peak values of periodic orbits become very large. With decreasing D the positive equilibrium becomes unstable and a stable limit cycle originates at the supercritical Hopf bifurcation H_3^- ($D = 0.03367$ h^{-1}). Observe that only the peak values are plotted. This limit cycle is continued and

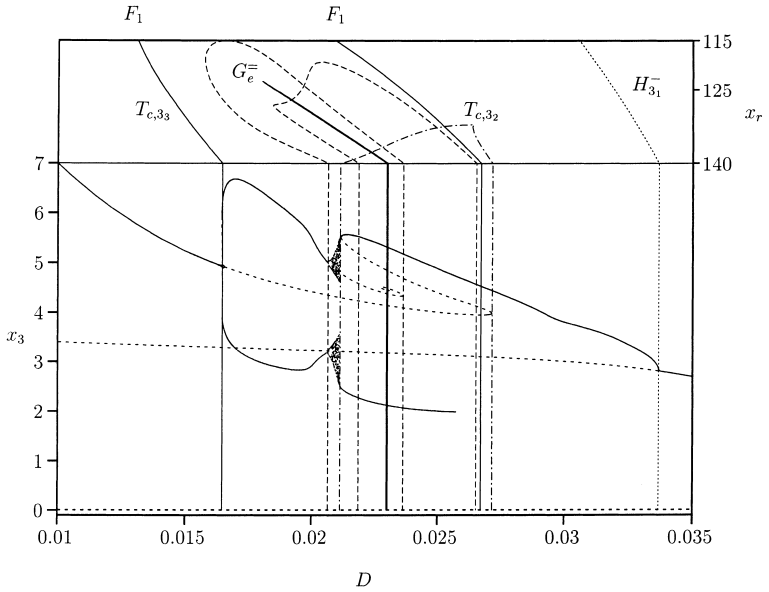

Fig. 8. One-parameter bifurcation diagram for the Droop model with peak (global and local) values of top predator x_3 [mg dm^{-3}]. The bifurcation parameter is the dilution rate D [h^{-1}]. The concentration in the reservoir is $x_r = 140$ mg dm^{-3}. Solid curves give stable equilibrium values and peak values of stable limit cycles. Dashed curves give unstable equilibrium values and (only global) peak values of unstable limit cycles. At the top the rotated two-parameter bifurcation diagram, Fig. 5, is plotted for $115 \leqslant x_r \leqslant 140$ mg dm^{-3}. Bifurcation points (the D values for intersection points in two-parameter diagram (Figs. 5 and 7) of bifurcation curves with $x_r = 140$ mg dm^{-3} line) are indicated by vertical lines.

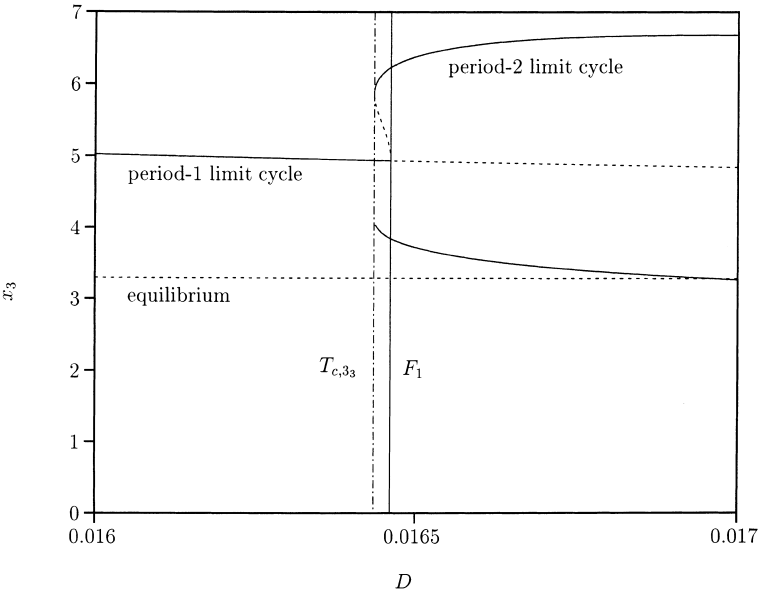

Fig. 9. One-parameter bifurcation diagram for the Droop model with peak (global and local) values of top predator close to the subcritical flip bifurcation F_1. This figure is an expanded picture of Fig. 8.

becomes unstable at the tangent bifurcation $T_{c,3_2}$ with $D = 0.02114\ \mathrm{h}^{-1}$. For $D = 0.02716\ \mathrm{h}^{-1}$ it becomes stable again and subsequently unstable at $D = 0.02672\ \mathrm{h}^{-1}$ at the flip bifurcation F_1. Finally it becomes stable again for $D = 0.01646\ \mathrm{h}^{-1}$ at the flip bifurcation F_1. This latter flip bifurcation is subcritical (see also [28], page 110). This means that, for a small interval around $D \approx 0.0165\ \mathrm{h}^{-1}$, in addition to the period-1 stable limit cycle, there is an unstable and a stable period-2 limit cycle. An expanded picture of Fig. 8 for the relevant D-values is shown in Fig. 9. These two period-2 limit cycles collide in the tangent bifurcation $T_{c,3_3}$ and disappear at that point with decreasing D. In the two-parameter bifurcation diagram (Fig. 9) there are two codimension 2 points, denoted as P_1 and P_2 at the flip bifurcation curve F_1 where the tangent bifurcation $T_{c,3_3}$ originates. The flip bifurcation F_1 transits in these points from subcritical, F_1^+, to supercritical F_1^- and vice versa. This means that near these points the difference between the peak values of the period-2 orbits increase very fast with the transition over the flip bifurcation curve.

Fig. 10 with $x_r = 150\ \mathrm{mg\ dm}^{-3}$ shows that the period-1 limit cycle originating at the Hopf bifurcation H_3^- which becomes unstable at the flip bifurcation F_2, is connected to the period-2 branch of the flip bifurcation F_1. Thus for the continuation with increasing D there is a supercritical flip bifurcation where the period-1 limit cycle becomes unstable. With decreasing D for a

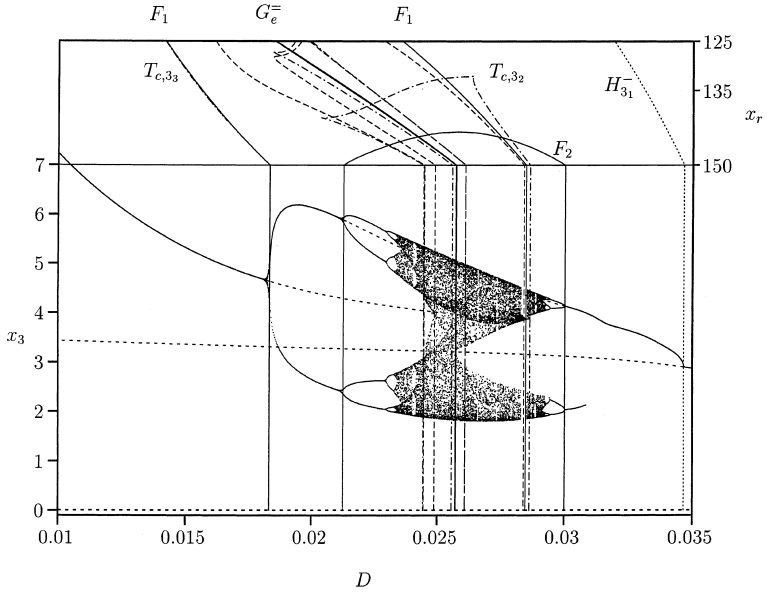

Fig. 10. One-parameter bifurcation diagram for the Droop model with peak (global and local) values of top predator x_3 [mg dm^{-3}]. The bifurcation parameter is the dilution rate D [h^{-1}]. The concentration in the reservoir is $x_r = 150$ mg dm^{-3}. Solid curves give stable equilibrium values and peak values of stable limit cycles. Dashed curves give unstable equilibrium values and (only global) peak values of unstable limit cycles. At the top the rotated two-parameter bifurcation diagram, Figs. 5 and 7, is plotted for $125 \leqslant x_r \leqslant 150$ mg dm^{-3}.

period-1 limit cycle one Floquet multiplier becomes 1 at the bifurcation point. This is, however, not a tangent bifurcation, as with $x_r = 140$ mg dm^{-3} (Fig. 8), but a pitchfork bifurcation for the second iterate of the unstable period-1 limit cycle. Kuznetsov ([28], page 110) shows that a flip bifurcation corresponds to a pitchfork bifurcation for the second iterate of a map in the case of a discrete-time system. Our case is associated with limit cycles of a continuous-time system.

4. Shil'nikov bifurcation

In this section the Shil'nikov bifurcation is discussed for the models with energy reserves, the Droop and DEB model first, and thereafter for the Marr–Pirt model. It is a global bifurcation for the unstable saddle-focus equilibrium. System (2a–2d) is seven-dimensional and the Jacobian matrix evaluated in the unstable equilibrium has one pair of complex conjugated eigenvalues with positive real parts while the other five eigenvalues are negative in the region of

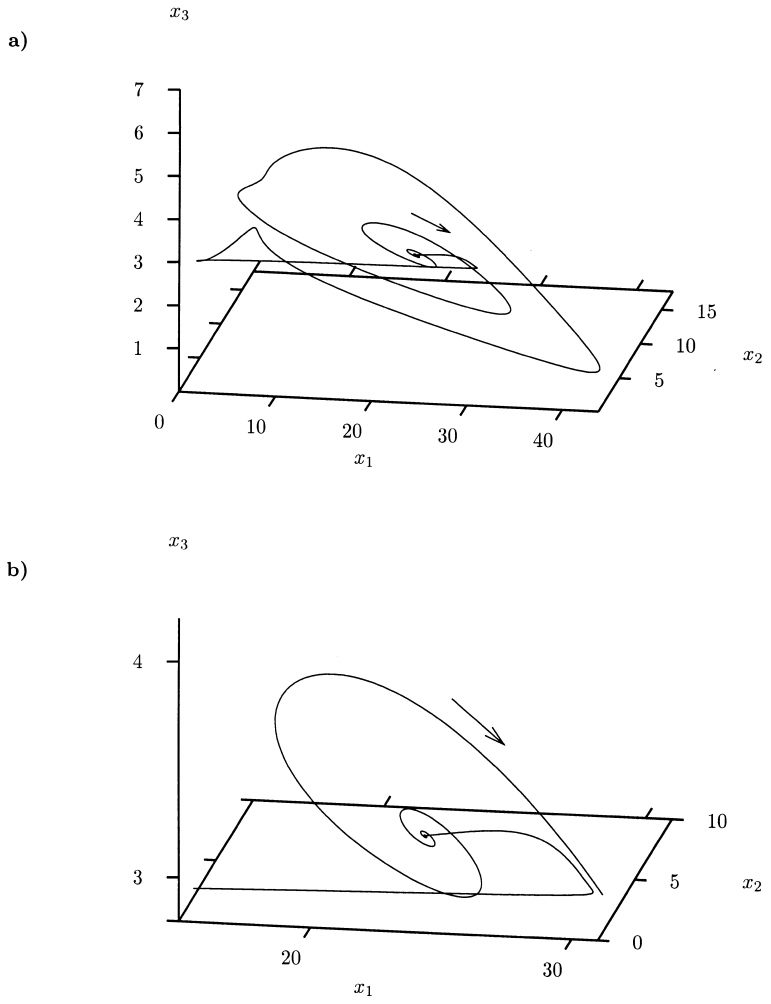

Fig. 11. (a) The homoclinic orbit for the Droop model with $D = 0.0180\text{h}^{-1}$ and $x_r = 123.2867$ mg dm^{-3}. (b) An expanded picture close to the saddle-focus equilibrium. The homoclinic orbit spirals outward along the two-dimensional unstable manifold and approaches the equilibrium along the one-dimensional stable manifold belonging to the leading negative eigenvalue.

the (x_r, D)-plane bounded by the Hopf bifurcation curve H_3^-. Moreover, the real eigenvalues have larger magnitude than the real parts of the complex conjugated eigenvalues. In these Shil'nikov bifurcations the homoclinic orbit spirals outward along the two-dimensional unstable manifold and approaches the equilibrium along the one-dimensional stable manifold corresponding to the leading negative eigenvalue closest to the imaginary axis (Fig. 11).

A one-parameter bifurcation diagram Fig. 12, where the period of the limit cycles denoted by T_0 is plotted against D with $x_r = 150$ mg dm^{-3}, illustrates that there seems to be a Shil'nikov bifurcation. By continuation of the period-1 limit cycles with increasing D a specific route of periodic solutions with period converging to infinity emerges converging to a homoclinic orbit associated with the saddle-focus equilibrium. At the homoclinic bifurcation the system has an infinite number of saddle limit cycles which originate each from a Smale horseshoe ([28], page 203). The first iterate limit cycle undergoes an infinite number of tangent bifurcations which become close to the homoclinic bifurcation point. At the branches where stable limit cycles originate from the tangent bifurcation, there are flip bifurcations where the limit cycle becomes unstable. These flip bifurcations generate double-period cycles. In Fig. 12 one second iterate is shown which also leads to a sequence of tangent and flip bifurcations with convergence to the homoclinic orbit similar to the first iterate.

The program HOMCONT being part of the AUTO package [24] is used for continuation of the homoclinic solution in the two-dimensional (x_r, D) parameter space. The theory is described in [29,34] and [28], page 467. As a starting strategy we used the data obtained by continuation with D as free parameter as describe above. That procedure, using AUTO, provides the data

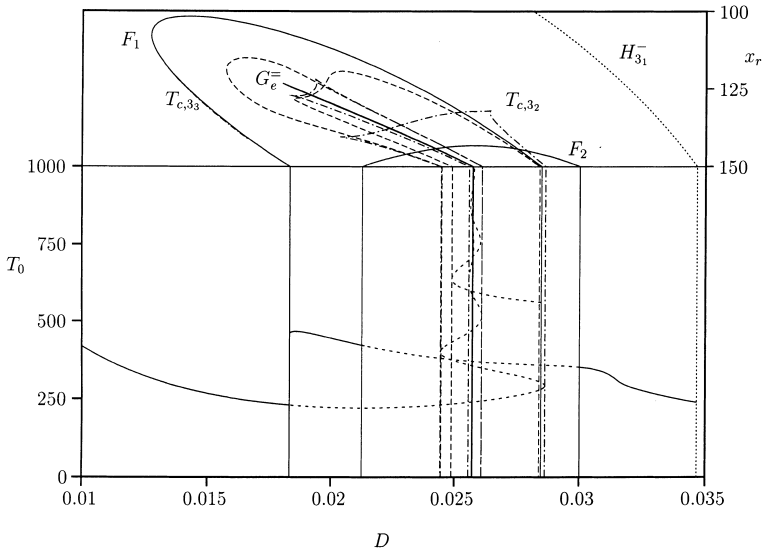

Fig. 12. One-parameter bifurcation diagram for the Droop model. The period, T_0 [h], is plotted as a function of dilution rate D [h^{-1}]. The concentration in the reservoir is $x_r = 150$ mg dm^{-3}. At the top the rotated two-parameter bifurcation diagram, Fig. 5, is plotted for $100 \leqslant x_r \leqslant 150$ mg dm^{-3}. Vertical lines indicate bifurcation points: the D values for intersection points in two-parameter diagram (Figs. 5 and 7) of bifurcation curves with $x_r = 150$ mg dm^{-3} line.

for the limit cycle with very large periods (in our case 4000 h). The final value of D is used to calculate the unstable equilibrium state values and the number of positive and negative eigenvalues at that point. The final limit cycle is used to calculate a better approximation for the homoclinic orbit.

One of the numerical approximations with the calculation of homoclinic orbits is the truncation of the infinite time-interval to a finite time interval $[-T, T]$ [29]. Using HOMCONT a better approximation for the homoclinic orbit is obtained with T and D as the free parameters. The time interval T is increased (in our case up to 20 000 h) while the equilibrium point is fixed at the approximative values. Finally this initial homoclinic orbit is continued in the two-dimensional parameter space with D and x_r as free parameters. The parameter T is now fixed. The calculated curve, denoted by $G_e^=$, is shown in Figs. 5 and 7 for the Droop model and in Fig. 6 for the DEB model.

Careful examination of the homoclinic bifurcation curve $G_e^=$ shows that there are two homoclinic curves very close to each other and indistinguishable in the two-parameter bifurcation diagrams. Hence, there is no codimension-two point, the curve 'turns' back similar to the flip bifurcation F_1 but with a very large curvature.

Fig. 13 displays the one-parameter bifurcation diagram for the Droop model where D and x_r change simultaneously along the homoclinic bifurcation curve $G_e^=$. Hence for all D values there is a homoclinic orbit for the saddle-focus equilibrium. Near to the turn point, with $D = 0.0180\ \mathrm{h}^{-1}$ and indicated by $G_e^=$, the local maxima during the chaotic orbits come very close to the equilibrium value of the top predator. Thus in this region there is coexistence of the chaotic attractor and a homoclinic orbit together with the associated stable limit cycles. At the intersection of the curve $G_e^=$ and curve $T_{c,3_2}$ there is a period-2 window, that is the chaotic attractor is cut by a limit cycle and we have coexistence of a period-2 stable limit cycle and a homoclinic orbit. When D is increased the chaotic region terminates when the tangent bifurcation $T_{c,3_2}$ intersects the chaotic attractor. When this tangent bifurcation is passed the homoclinic orbit together with the associated stable limit cycles are the interior solutions.

In Fig. 13 also the maxima for the top predator are shown for $D < 0.0180\ \mathrm{h}^{-1}$. The curve $G_e^=$ is extended by a line starting at the extreme point calculated with HOMCONT. By increasing the D along this line from the point denoted by F_1 which indicates the first period doubling, a cascade of period doubling leads to chaotic behaviour.

With the Marr–Pirt model we had to follow a different starting strategy. We were not able to continue a limit cycle where the period becomes very large. A shooting method was used to find a starting point. The fact that a homoclinic orbit is fixed by the position where a chaotic attractor touches the unstable equilibrium was used. One-parameter plots for the Marr–Pirt model already given in [30], which are similar to those given in the present paper, indicated positions in the parameter space where a homoclinic orbit could exist. With

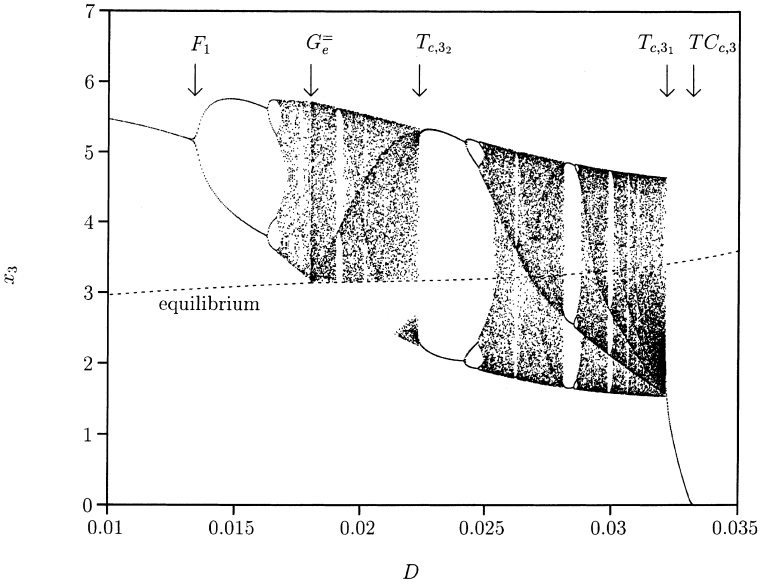

Fig. 13. One-parameter bifurcation diagram for Droop model with peak (global and local) values of the top predator. The bifurcation parameters, the dilution rate D [h^{-1}] and the concentration in reservoir is x_r [mg dm^{-3}] are adjusted in order that we follow the homoclinic curve $G_e^=$ in Fig. 5. Solid curves give stable equilibrium values and peak values of stable limit cycles. Dashed curves give the unstable equilibrium values for x_3 [mg dm^{-3}].

HOMCONT the time interval T was increased yielding a homoclinic orbit. This orbit was used with the continuation of the codimension 1 homoclinic bifurcation. The result is the curve $G_e^=$ already shown in Fig. 4.

The homoclinic bifurcation curve was also calculated with a technique similar to the one presented in [30] for the calculation and continuation of global bifurcations. These global bifurcations are homoclinic orbits for the unstable limit cycle which originates with the supercritical Hopf bifurcation H_3^+ and heteroclinic orbits between this cycle and the equilibrium. Both continuation techniques gave almost the same results, although HOMCONT is a general purpose program whereas the implementation of the method proposed in [30] makes use of some special features of the four-dimensional system (3a–3d).

The Monod model, being the Marr–Pirt model with no maintenance ($m_i = 0, i = 1, 2, 3$) seems to have no homoclinic bifurcation curve in the region of the parameter space considered here. This was shown as follows. Starting with the Marr-Pirt model at the boundary of the parameter space, $x_r = 300$ mg dm^{-3}, continuation with first m_3 and subsequently with m_1 yielded a homoclinic orbit with $m_1 = m_3 = 0$ and $m_2 = 0.01$ h^{-1}. Continuation with m_2 as one of the free parameters revealed that this parameter continued to be positive.

5. Discussion and conclusions

The global picture of the bifurcation diagrams of all models (Figs. 3–6) are the same. Enrichment of the food chain leads for the bi-trophic food chain to cyclic dynamic behaviour. For a tri-trophic food chain persistence is possible only in a relatively small region of the control parameter space, while complex, including chaotic, dynamic behaviour can occur. A codimension 2 point (denoted by M_1) acts as the 'organizing center' where the bifurcation points for the tri-trophic food chain originate. We want to stress that for other parameter values the bifurcation diagrams are different from those presented in this paper but the general picture will be about the same.

The extensions of the Monod model concern maintenance and energy reserves as is summarized in Table 1. The importance of these two quantities follow from:

Maintenance: Influences strongly the dynamic behaviour for low dilution rates. With maintenance all population except the prey are washed-out at small dilution rates. Maintenance gives a somewhat smaller region of persistence of the whole food chain.

Energy reserves: Influences the dynamic behaviour for large dilution rates and gives coexistence of stable limit cycles. Energy reserves yield a much smaller region in the bifurcation diagram where the tri-trophic food chain persists.

Although the global picture of the bifurcation diagrams of all models resemble each other, there are considerable differences with respect to the precise positions of the bifurcations curves. These can help to distinguish between models when experimental data about the asymptotic behaviour are available. Suppose that parameters are estimated from experimental short-term time-course data for each model. Then, using these fixed parameter values, points in the bifurcation diagrams can be found where the models predict a pronounced different dynamical behaviour, for instance one model predicts wash-out of the predator and another does not. Then with these parameter settings a number of additional experiments can be performed. When for one model the predicted long-term behaviour is also observed in contrast to that for the other models, this model is best suited.

In a previous paper [35] we studied the dynamic behaviour of the system when the scaled energy reserves density equals the scaled functional response $e_i(t) = f_{i-1,i}(t)$, $i = 1, 2, 3$. This is justified when the parameters $v_{i-1,i}$, $i = 1, 2, 3$ in (2d) are relatively large. In that way a reduction of the state space dimension from seven to four is obtained by a singular perturbation argument. The assumption that the reserves change quasi-statically has no influence on the transcritical bifurcations curves for the equilibria. Comparison of the bifurcation diagram, Fig. 6, with the diagram presented in [35] reveals that, with the parameter values given in Table 4, the dynamics of the reserves themselves are

important in the study of the long-term behaviour of limit cycles and more complex dynamic behaviour. In conclusion, it is advisable to solve the full system.

In [30] other global bifurcations for the Marr–Pirt model are described. These global bifurcations are homoclinic as well as heteroclinic for an unstable limit cycle. A discussion of these global bifurcations is beyond the scope of this paper. In the present paper only global bifurcations to the unstable interior equilibrium are considered.

The importance of the global bifurcations is the connection with chaotic behaviour. Klebanoff and Hastings [9] studied the normal form of a bifurcation point M_1 in the Rosenzweig–MacArthur model. They associated the origin of chaos with this bifurcation point. Kuznetsov and Rinaldi [10] showed that chaos arises in a region far from M_1 of the parameter space. This is also the case for the four mass-balance models. Furthermore homoclinic orbits of the Shil'nikov type were shown to be related to a strange attractor in [5]. In [36] a singular perturbation analysis was used to prove that the Rosenzweig–MacArthur model possesses a homoclinic bifurcation. In the present paper it is shown numerically that for the mass-balance model a homoclinic bifurcation for a saddle-focus equilibrium forms the skeleton of the cascade of period doubling which leads to chaotic behaviour (see for instance Fig. 7).

Acknowledgements

The authors like to thank Eusebius Doedel and Yuri Kuznetsov for valuable discussions, Hugo van den Berg and Wim van der Steen for corrections in the manuscript. The research of the second author was supported by the Netherlands Organization for Scientific Research (NWO).

References

[1] O. De Feo, S. Rinaldi, Yield and dynamics of tritrophic food chains, Am. Natur. 150 (1997) 328.
[2] M.L. Rosenzweig, R.H. MacArthur, Graphical representation and stability conditions of predator-prey interactions, Am. Natur. 97 (1963) 209.
[3] M.L. Rosenzweig, Exploitation in three trophic levels, Am. Natur. 107 (1973) 275.
[4] P.A. Abrams, J.D. Roth, The effects of enrichment of three-species food chains with nonlinear functional responses, Ecology 75 (1994) 1118.
[5] K. McCann, P. Yodzis, Bifurcation structure of a tree-species food chain model, Theoret. Population. Biol. 48 (1995) 93.
[6] P. Yodzis, S. Innes, Body size consumer-resource dynamics, Am. Natur. 139 (1992) 1151.
[7] A. Hastings, T. Powell, Chaos in a three-species food chain, Ecology 72 (1991) 896.

[8] A. Klebanoff, A. Hastings, Chaos in one-predator, two-prey models: General results from bifurcation theory, Math. Biosci. 122 (1994) 221.
[9] A. Klebanoff, A. Hastings, Chaos in three-species food chain, J. Math. Biol. 32 (1994) 427.
[10] Y.A. Kuznetsov, S. Rinaldi, Remarks on food chain dynamics, Math. Biosci. 124 (1996) 1.
[11] A. Gragnani, S. Rinaldi, A universal bifurcation diagram for seasonally perturbed predator-prey models, Bull. Math. Biol. 57 (1995) 701.
[12] J. Monod, Recherches sur la croissance bactériennes, Hermann, Paris, 1942.
[13] D. Herbert, Some principles of continuous culture, in: G. Tunevall, (Ed.), Recent progress in Microbiology, Blackwell, Oxford, England, 1958, pp. 381.
[14] M.R. Droop, Some thoughts in nutrient limitation in algae, J. Phycol. 9 (1973) 264.
[15] K. Lange, F.J. Oyarzun, The attractiveness of the Droop equations, Math. Biosci. 111 (1992) 261.
[16] S.A.L.M. Kooijman, Dynamic Energy Budgets in Biological Systems; Theory and Applications in Ecotoxicology, Cambridge University, Cambridge, 1993.
[17] B.W. Kooi, S.A.L.M. Kooijman, Existence and stability of microbial prey-predator systems, J. Theoret. Biol. 170 (1994) 75.
[18] J.A.J. Metz, O. Diekmann, The dynamics of physiologically structured populations, volume 68 of Lecture Notes in Biomathematics, Springer, Berlin, 1986.
[19] A. Cunningham, R.M. Nisbet, Transients and oscillations in continuous culture, in: M.J. Bazin, (Ed.), Mathematical Methods in Microbiology, 1983, pp. 77.
[20] R.M. Nisbet, A. Cunningham, W.S.C. Gurney, Endogenous metabolism and the stability of microbial prey-predator systems, Biotechnol. Bioeng. 25 (1983) 301.
[21] M. Kot, G.S. Sayler, T.W. Schultz, Complex dynamics in a model microbial system, Bull. Math. Biol. 54 (1992) 619.
[22] S. Pavlou, I. Kevrekidis, Microbial predation in a periodically operated chemostat: A global study of the interaction between natural and externally imposed frequencies, Math. Biosci. 108 (1992) 1.
[23] E. Doedel, J. Kernévez, Auto: Software for continuation problems in ordinary differential equations with applications, Technical report, California Institute of Technology, Applied Mathematics, 1986.
[24] E.J. Doedel, A.R. Champneys, T.F. Fairgrieve, Y.A. Kuznetsov, B. Sandstede, X. Wang, Auto 97: Continuation and bifurcation software for ordinary differential equations, Technical report, Concordia University, Montreal, Canada, 1997.
[25] A.I. Khibnik, Y.A. Kuznetsov, V.V. Levitin, E.V. Nikolaev, Continuation techniques and interactive software for bifurcation analysis of ODEs and iterated maps, Physica D 62 (1993) 360.
[26] J. Guckenheimer, P. Holmes, Nonlinear Oscillations, Dynamical Systems and Bifurcations of Vector Fields, volume 42 of Applied Mathematical Sciences, 2nd ed., Springer, Berlin, 1985.
[27] S. Wiggins, Introduction to Applied Nonlinear Dynamical Systems and Chaos, volume 2 of Texts in Applied Mathematics, Springer, New York, 1990.
[28] Y.A. Kuznetsov, Elements of Applied Bifurcation Theory, volume 112 of Applied Mathematical Sciences, Springer, New York, 1995.
[29] A. Champneys, Y.A. Kuznetsov, B. Sandstede, A numerical toolbox for homoclinic bifurcation analysis, Int. J. Bifurcation Chaos 6 (1995) 867.
[30] M.P. Boer, B.W. Kooi, S.A.L.M. Kooijman, Food chain dynamics in the chemostat, Math. Biosci. 150 (1998) 43.
[31] S.J. Pirt, The maintenance energy of bacteria in growing cultures, Proc. Roy. Soc. London B 163 (1965) 224.
[32] H.L. Smith, P. Waltman, The Theory of the Chemostat, Cambridge University, Cambridge, 1994.

[33] B.W. Kooi, M.P. Boer, S.A.L.M. Kooijman, Mass balance equation versus logistic equation in food chains, J. Biol. Systems 5 (1997) 77.
[34] A. Champneys, Y.A. Kuznetsov, Numerical detection and continuation of codimension-two homoclinic bifurcations, Int. J. Bifurcation Chaos 4 (1994) 795.
[35] B.W. Kooi, M.P. Boer, S.A.L.M. Kooijman, Complex dynamic behaviour of autonomous microbial food chains, J. Math. Biol. 36 (1997) 24.
[36] O. De Feo, S. Rinaldi, Singular homoclinic bifurcations in tri-trophic food chains, Math. Biosci. 148 (1998) 7.